We are IntechOpen, the world's leading publisher of Open Access books Built by scientists, for scientists

6,900
Open access books available

186,000
International authors and editors

200M
Downloads

154
Countries delivered to

Our authors are among the
TOP 1%
most cited scientists

12.2%
Contributors from top 500 universities

CLARIVATE ANALYTICS
BOOK CITATION INDEX
INDEXED

WEB OF SCIENCE™

Selection of our books indexed in the Book Citation Index
in Web of Science™ Core Collection (BKCI)

Interested in publishing with us?
Contact book.department@intechopen.com

Numbers displayed above are based on latest data collected.
For more information visit www.intechopen.com

Chapter

Porous ZnO Nanostructures Synthesized by Microwave Hydrothermal Method for Energy Harvesting Applications

Sofia Henriques Ferreira, Ana Rovisco,
Andreia dos Santos, Hugo Águas, Rui Igreja,
Pedro Barquinha, Elvira Fortunato and Rodrigo Martins

Abstract

The ever-growing global market for smart wearable technologies and Internet of Things (IoT) has increased the demand for sustainable and multifunctional nanomaterials synthesized by low-cost and energy-efficient processing technologies. Zinc oxide (ZnO) is a key material for this purpose due to the variety of facile methods that exist to produced ZnO nanostructures with tailored sizes, morphologies, and optical and electrical properties. In particular, ZnO nanostructures with a porous structure are advantageous over other morphologies for many applications because of their high specific surface area. In this chapter, a literature review on the latest progress regarding the synthesis and applications of ZnO with a porous morphology will be provided, with special focus on the synthesis by microwave hydrothermal method of these nanomaterials and their potential for application in energy harvesting devices. Nanogenerators of a composite made by polydimethylsiloxane (PDMS) and porous ZnO nanostructures were explored and optimized, with an output voltage of (4.5 ± 0.3) V being achieved for the best conditions. The daily life applicability of these devices was demonstrated by lighting up a commercial LED, by manually stimulating the nanogenerator directly connected to the LED.

Keywords: zinc oxide, microwave synthesis, porous nanostructures, energy harvesting devices

1. Introduction

Zinc oxide (ZnO) is an inorganic semiconductor material that has been applied in a wide range of applications over the last centuries [1]. The attraction to ZnO can be attributed to its remarkable optical and electronic characteristics. With a direct and wide bandgap of 3.37 eV and a large exciton binding energy of 60 meV at room temperature [2], ZnO has the potential to be applied in advanced electronic and optoelectronic devices with promising results, such as UV sensors [3, 4], transparent electrodes [5, 6], gas sensors [7], thin film transistors [8, 9], and solar cells [10–12].

Moreover, ZnO is a low-cost and biocompatible material with high photostability, high chemical and thermal stability, low toxicity, and a broad range of UV radiation absorption [13]. These properties allow ZnO to be applied in a wide range of applications besides electronic devices, such as skin ointments and sunscreens, rubber tires, paints, bioimaging, drug delivery, biosensors, antibacterial textiles, and photocatalysis for the degradation of pollutants in wastewaters [1, 14–19].

Due to its piezoelectric properties, ZnO nanostructures have also been widely explored for energy harvesting applications, being an important sustainable energy source [20]. The demand for wearable devices led to a high development of new energy sources. Nanogenerators have demonstrated the capability to power small electronic devices, appearing as a good alternative to batteries [21]. The most common nanogenerators are based on piezoelectric and/or triboelectric effects. In the piezoelectric nanogenerators, mechanical energy is converted into electrical energy through piezoelectric polarization resultant from strain [1]. The triboelectric effect results from the surface charges' generation subsequent from the friction between two different materials (with opposite triboelectric polarities) [22].

Materials with piezoelectric properties have the capability to convert mechanical energy into electrical energy [1]. Within the different piezoelectric materials, lead zirconate titanate (PZT) is the material that presented so far the highest piezoelectric coefficient (d_{33} = 593 pC N^{-1}), still this material has a high toxicity [23, 24]. While presenting a much lower d_{33} value($\approx$ 10 pC N^{-1}) [25–27], ZnO is a very good alternative, since it is not only sustainable and eco-friendly, as it can also be easily fabricated, while still presenting a good performance [28, 29].

Nanogenerators of different types of ZnO nanostructures (i.e., nanorods, nanoparticles, nanoflowers) have been reported [30–34]. For example, Saravanakumar et al. reported a nanogenerator fabricated using vertically grown ZnO nanowires with surrounding PDMS, with output values of 6 V/4 nA/0.39 nW cm^{-2} under finger bending [35]. Rahman et al. used ZnO nanoparticles dispersed into a PDMS film, achieving output values of 20 V/20 μA/20 μW, with finger tapping [36]. As another example, ZnO nanoflowers were mixed with multiwalled carbon nanotubes and PDMS, with an output of 75 V/3.2 μA/260 mW cm^{-2} being obtained. In this case, the devices were tested in the soles of human shoes with the force being applied by a person walking [37].

1.1 Synthesis and applications of porous ZnO nanostructures

Despite all the established applications of ZnO, the research involving this semiconductor has not yet diminished, mostly due to the continuing development of new synthesis technologies and applications. For instance, ZnO nanomaterials can be easily synthesized into tailored sizes and morphologies at low temperatures (< 200 °C) by a variety of methods, including chemical bath deposition [38], electrodeposition [39], chemical vapor deposition [40], electrospinning [41], laser assisted flow deposition [42], and solvothermal [16] or hydrothermal [43, 44] synthesis, either by conventional or microwave-assisted heating [4, 45].

Porous oxide semiconductor nanomaterials, particularly two-dimensional (2D) materials with nanoscale thickness, are promising candidates due to their usually large specific surface areas that can improve their performance in several applications [46–51]. These nanomaterials can inclusively assemble into three-dimensional (3D) hierarchically structures with controlled morphology and dimensions which can lead to novel properties and applications [52]. The self-assemble technique is a facile method to produce 3D hierarchical structures where low-dimension building units aggregate spontaneously into high-dimensional architectures. This technique

offers many advantages over other methods as it can be performed at low temperatures using low-cost materials while having high yield for scale production [52].

An indirect way to produce porous 3D ZnO structures has been recently developed by thermal decomposition of layered zinc hydroxide (LZH) precursors [52]. LZHs are usually composed of positively charged zinc hydroxyl layers intercalated by anions that balance the overall charge and water molecules [53]. The anions in LZH generally include CO_3^{2-}, SO_4^{2-}, NO_3^-, Cl^-, CH_3COO^- [50, 53–58]. These LZH precursors are fabricated with the desired morphology and then converted into porous ZnO nanomaterials by a calcination process at high temperatures [59]. During calcination, the precursors release gaseous molecules and, consequently, the original structure contracts and pores are formed throughout the structures [52].

LZHs are typically obtained via solution techniques, mainly hydrothermal methods where the materials' synthesis occurs in a basic medium that results from the addition of certain reagents, such as hexamethylenetetramine [60], ammonia [58, 61], and urea [52, 62–65]. Although the basic structure is similar in all LZHs, the sites occupied by the anions and water molecules are different and, as a result, the final morphology, crystal structure, interlayer distances, and thermal decomposition temperature differ depending on the anion type [66]. In particular, the LZH carbonate (LZHC) is composed of zinc hydroxide layers combined with carbonate ions and water molecules. During the synthesis of this material, a well-crystallized phase is typically obtained with an invariable distance between the LZH [53]. The resulting morphology of LZHC usually consists of 2D structures stacked in a hierarchical 3D arrangement. However, the synthesis of uniform LZHC 3D morphologies through a simple and fast hydrothermal method has not yet been fully explored.

For this purpose, hydrothermal synthesis assisted by microwave irradiation offers many advantages over conventional heating. In a synthesis assisted by conventional heating, the heat transfer occurs through a combination of conductive and convective mechanisms that result in a low heating rate and, consequently, long synthesis time [67]. Conventional heating method is also dependent on the thermal conduction of the material of which the reaction vessel walls are made. Moreover, the temperature maximum occurs on the vessel wall surface, as shown in **Figure 1**. All these factors can lead to a non-uniform heating of the reaction medium and, subsequently, originate a heterogeneity in the obtained products [1]. On the other hand, hydrothermal synthesis assisted by microwave irradiation allows for rapid and uniform heating since the heat transfer occurs directly from the microwaves to the molecules of the reaction's materials, as illustrated in **Figure 1**. This results in high reaction rates and a homogeneous and volumetric heating [68, 69].

The porous morphology of ZnO nanostructures obtained by calcination of LZHC significantly increases the materials' specific surface area [70] and, therefore,
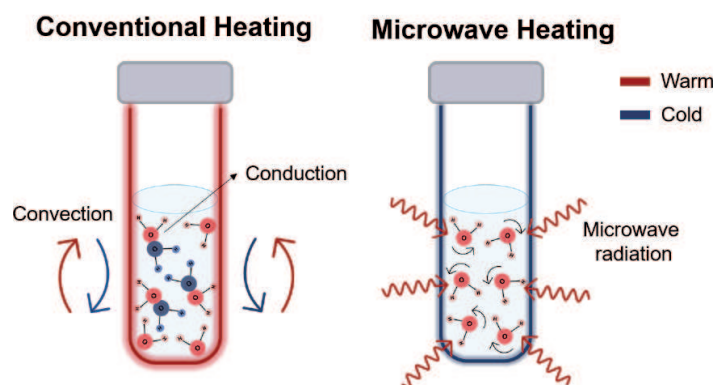

Figure 1.
Schematic of conventional heating versus microwave heating processes.

these ZnO nanomaterials have been used in applications that benefit from this characteristic, such as photocatalysis [51, 52, 70], gas sensors [50, 54, 71–73], surface enhanced Raman scattering (SERS) substrates [74], dye-synthesized solar cells [44, 75, 76], and battery electrodes [65].

This work aims to demonstrate the potential of high surface area porous ZnO nanostructures for energy harvesting devices, showing original and novel results regarding the characterization of nanogenerators based on these structures. For that, 3D hierarchically structures composed of LZHC nanoplates were successfully synthesized through a facile, low-cost, and low temperature hydrothermal process assisted by microwave irradiation. Porous ZnO nanostructures were obtained by calcination of the LZHC at 700 °C for 2 h in air while maintaining the LZHC hierarchical 3D structure. Porous ZnO nanostructures were then embedded in PDMS and deposited by spin-coating technique on flexible substrates. Energy harvesting based on a micro-structured composite of porous ZnO nanostructures embedded in PDMS was investigated. The combination of using the porous ZnO nanostructures, which have piezoelectric properties, and triboelectricity resultant from the micro-structuring leads to a performance improvement of the nanogenerators [37, 77]. To the best of our knowledge, porous ZnO nanostructures were for the first time used to fabricate a micro-structured PDMS/ZnO composite for energy harvesting devices.

2. Materials and methods

2.1 Synthesis and characterization of porous ZnO nanostructures

Porous ZnO nanostructures were synthesized by hydrothermal method assisted by microwave irradiation. Zinc nitrate hexahydrate ($Zn(NO_3)_2 \cdot 6H_2O$, Sigma-Aldrich 98%) and urea (CH_4N_2O, Sigma-Aldrich 99.0–100.5%) were used without further purification. In a typical synthesis, 0.05 M of zinc nitrate was first dissolved in de-ionized water, and after its total dissolution, urea was added to the aqueous solution. The molar ratio of zinc to urea was kept at 1:5. Then, 25 mL of the obtained solution was transferred to a 35 mL Pyrex vessel which was placed in a CEM Discovery SP microwave. The synthesis was carried out at 140 °C for 15 min under a power of 100 W.

After the synthesis, the resulting white precipitates were washed with de-ionized water followed by isopropanol and centrifuged at 4500 rpm for 5 min. This washing process was repeated three times. The powders were dried in air at room temperature for 48 h and then calcinated in air in a Nabertherm muffle furnace at 700 °C for 2 h with a heating rate of 250 °C h^{-1}.

The crystallinity of the produced nanostructures was analyzed by X-ray diffraction (XRD) using a PANalytical's X'Pert PRO MRD X-ray diffractometer, with a monochromatic Cu Kα radiation source with wavelength 1.540598 Å. XRD measurements were carried out from 10 to 90° (2θ), with a scanning step size of 0.016°. The morphology of the LZHC precursor and porous ZnO nanostructures was evaluated by scanning electron microscopy (SEM) using a Carl Zeiss AURIGA CrossBeam FIB-SEM workstation equipped with an Oxford X-ray Energy Dispersive Spectrometer.

Differential scanning calorimetric (DSC) and thermogravimetry (TG) measurements of the synthesized product without any temperature treatment were carried out with a simultaneous thermal analyzer NETZSCH STA 449 F3 Jupiter. Approximately 20 mg of the synthesized powder was loaded into an open platinum-rhodium crucible and heated in air from room temperature to 850 °C with a heating rate of 10 °C min^{-1}.

Diffuse reflectance measurements of the porous ZnO nanostructures were performed at room temperature using a PerkinElmer lambda 950 UV/VIS/NIR spectrophotometer with a diffuse reflectance module with a 150 mm diameter integrating sphere, internally coated with Spectralon. The calibration of the system was achieved by using a standard Spectralon reflector sample as reference. The reflectance spectra were obtained from 350 to 800 nm.

2.2 Fabrication and characterization of energy harvesting devices

The devices were fabricated as described in references [27, 78] and the fabrication process is illustrated in **Figure 2**. Briefly, composites of porous ZnO nanostructures embedded in PDMS were produced with concentrations of 20, 25, and 30 wt%. Firstly, the nanostructures were mixed with the PDMS elastomer (from Dow Corning) and a volume of ethyl acetate (from Fluka-Honeywell) enough to ensure a homogeneous mixture of elastomer and nanostructures. The mixture was stirred until the evaporation of the solvent, and then a curing agent (Sylgard 184, from Dow Corning) was added in a weight ratio to the elastomer of 1:10 while stirring to obtain a homogeneous mixture. Two types of devices were produced, unstructured and micro-structured nanogenerators. The former was fabricated by spin-coating the mixture at 250 rpm for 90 s, with an acceleration of 100 rpm·s^{-1}, on commercial substrates of polyethylene terephthalate (PET) with a layer of indium tin oxide (ITO) deposited on top (PET/ITO, from Kintec Company), whereas the latter was obtained by depositing the mixture in a similar way on acrylic molds (5 mm thick, from Dagol). The acrylic molds used were produced as described in reference [79].

The composites were then cured at 60 °C for 1 h. After the curing process, PET/ITO electrodes were placed on top of the composite films, as shown in **Figure 2**. The electrical characterization of the produced nanogenerators was performed by applying a mechanical stimulus in a contact area of 0.3 cm^2 with a pushing force of 2.3 N at different frequencies (0.5, 1, 1.5, and 2 pushes per second) with a home-made machine with a linear motor.
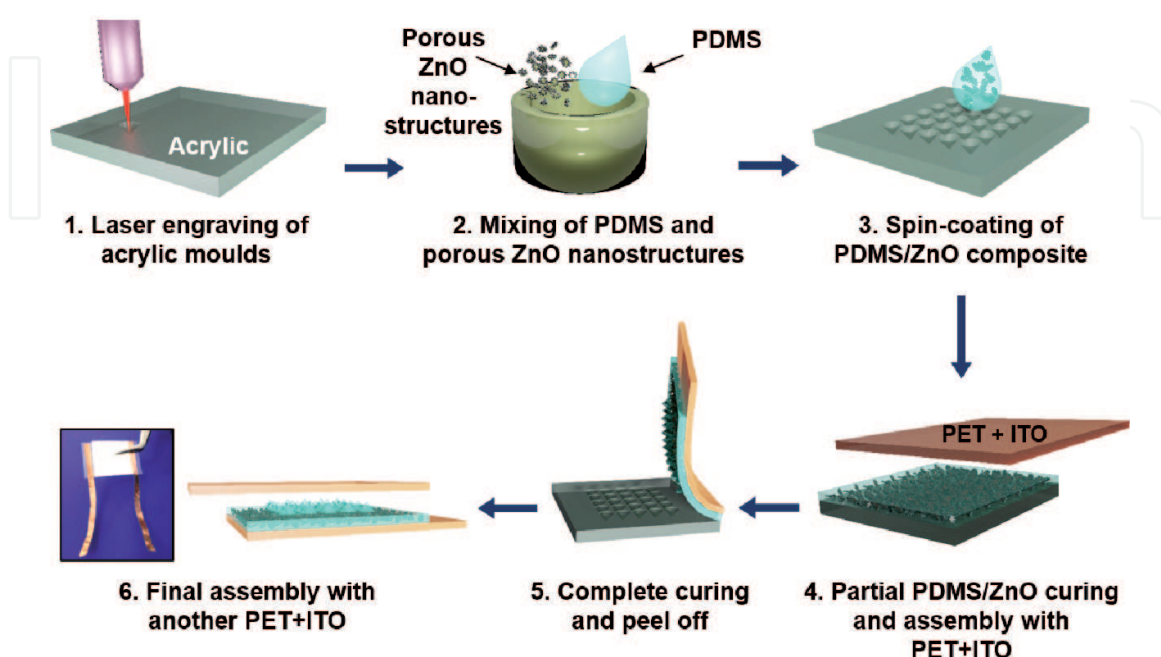

Figure 2.
Fabrication schematic of a micro-structured nanogenerator based on a PDMS/ZnO composite film. Adapted from dos Santos et al. [78].

3. Porous ZnO nanostructures as a piezoelectric material for nanogenerators

3.1 Synthesis of porous ZnO nanostructures

3.1.1 Characterization of the LZHC precursor

Figure 3(a) presents the X-ray diffractogram obtained from the final product of the hydrothermal synthesis prior to the calcination process. All the peaks from the diffractogram can be indexed to zinc hydroxide carbonate hydrate ($Zn_4(CO_3)$ $(OH)_6 \cdot H_2O$) (ICDD 11–0287). The morphology of the precursor was observed in SEM and it is shown in **Figure 3(b)**. The SEM image reveals that the LZHC precursor obtained after only 15 min of microwave hydrothermal synthesis consists of many flower-like structures, with a few micrometers of diameter, composed of densely packed LZHC nanoplates with a few nanometers of thickness.

Differential scanning calorimetric (DSC) measurements were carried out in air from room temperature to 800 °C to analyze the conversion process of LZHC into ZnO. The DSC curve in **Figure 3(c)** shows two endothermic peaks at 64 °C and 266 °C. The peak at 64 °C corresponds to the removal of water that is weakly adsorbed to the LZHC nanostructures [80], resulting in a weight loss of 38.12%. The second peak at 266 °C results in a weight loss of 14.87% and it is associated with the release of water and carbon dioxide from the thermal decomposition of LZHC precursor [50, 59].

3.1.2 Characterization of the porous ZnO nanostructures

After the calcination process, the LZHC precursor was successfully converted into porous ZnO nanostructures, which can be inferred from the X-ray diffractograms of the samples obtained at 700 °C, depicted in **Figure 4(a)**. All the peaks in the diffractogram correspond to the hexagonal wurtzite ZnO structure (ICDD 36–1451). No characteristic peaks from any other impurities were detected, indicating that the LZHC precursor was completely converted into ZnO. SEM images of the calcinated product are presented in **Figure 4(b)** with different magnifications. The low magnification image shows that the morphology of the final ZnO product did not suffer significant changes when compared with the LZHC precursor, since ZnO nanoplates are still assembled into flower-like structures. However, when observing the high magnification SEM images, it is possible to see that the ZnO nanoplates present a porous structure with serrate edges and a wide pore size distribution.

The synthesis of LZHC precursor by urea-assisted hydrothermal method, followed by the calcination process to originate porous ZnO nanostructures, has been explained before in the literature [44, 65, 73, 80, 81]. **Figure 5** shows a simple schematic of the synthesis and transformation process of LZHC precursor into porous ZnO nanostructures. During the hydrothermal synthesis, urea is hydrolyzed leading to the formation of hydroxide (OH^-) and carbonate (CO_3^{2-}) ions. Zn^{2+} ions from the added zinc salt react with both OH^- and CO_3^{2-} ions forming the LZHC precursor ($Zn_4(CO_3)(OH)_6 \cdot H_2O$). It has been reported that the surface of LZHC plates is hydrophobic whereas the lateral sides are hydrophilic, resulting in a vertical growth of this material and consequent plate-like morphology [76, 82, 83]. The agglomeration of these nanoplates into stable flower-like microstructures occurs to favor the minimization of surface energy by reducing exposed surface areas [83]. Under calcination at high temperature, LZHC is decomposed into ZnO by releasing
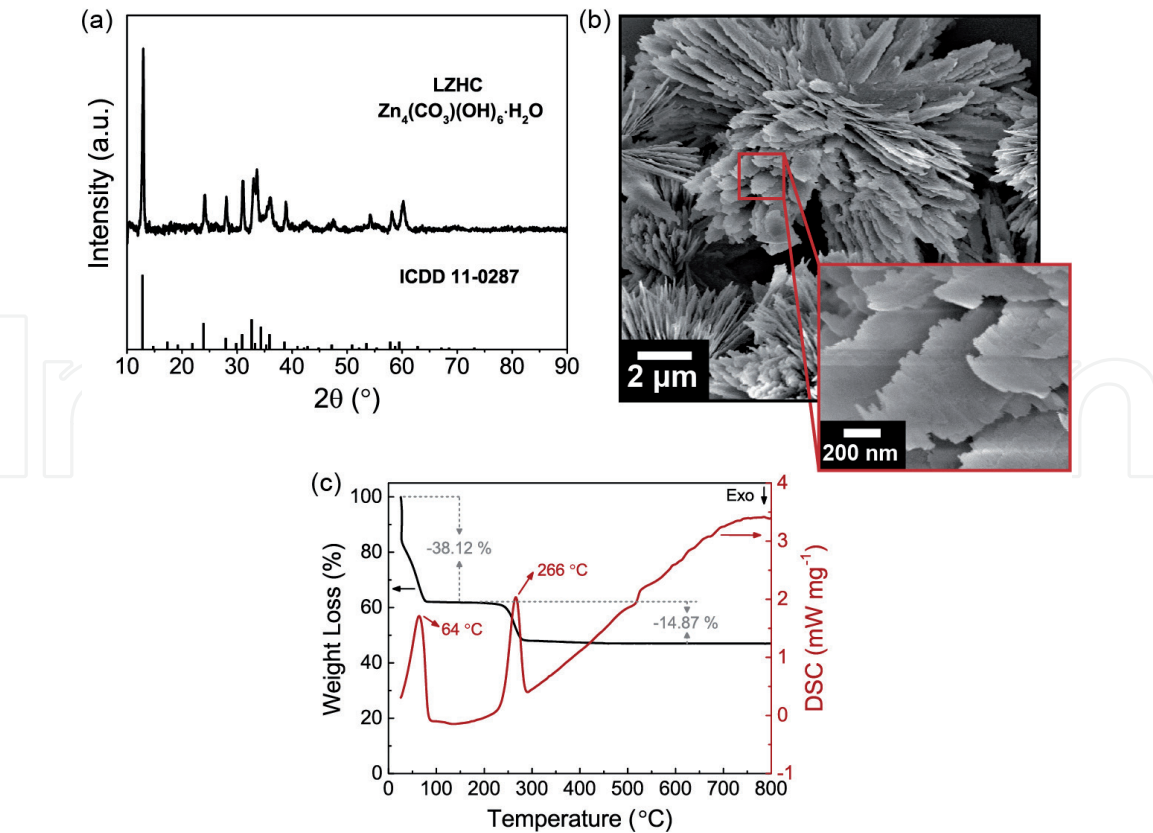
Figure 3.
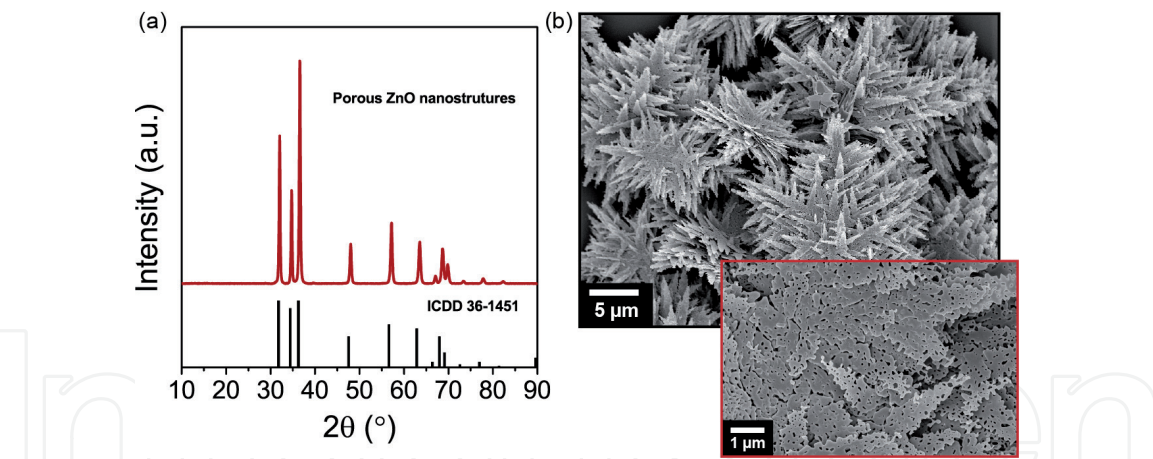*(a) X-ray diffractogram, (b) SEM images and (c) TG/DSC curves of the LZHC precursor.*

Figure 4.
(a) XRD diffractogram and (b) SEM images of porous ZnO nanostructures synthesized by hydrothermal method assisted by microwave irradiation followed by calcination at 700 °C for 2 h in air.

H_2O and CO_2 in the form of gas, which leads to a contraction of the original structure which originates pores throughout the nanoplates and a consequent porous ZnO structure, as illustrated in **Figure 5** [84].

The UV–Vis diffuse reflectance of the produced ZnO samples is presented in **Figure 6**. The optical band gap E_g was calculated by applying the Kubelka-Munk (K-M) method to the reflectance (R) data [85]. The K-M method is based on the following equation:

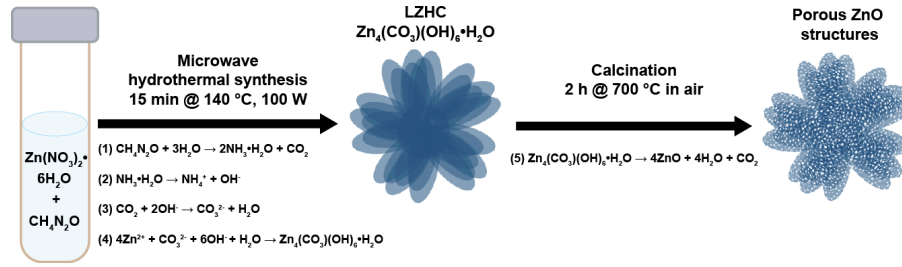$$F(R) = \frac{(1-R)^2}{2R} \tag{1}$$

Figure 5.
Schematic of the hydrothermal synthesis assisted by microwave irradiation and calcination process of porous ZnO structures.

The K-M function $(F(R))$ is proportional to the absorption coefficient (α). Therefore, by considering the Tauc relation, the following expressions can be obtained [86]:

$$F(R) \propto \alpha \propto = \frac{\left(h\upsilon - E_g\right)^{1/n}}{h\upsilon} \qquad (2)$$

$$\left(F(R)h\upsilon\right)^{n} = A\left(h\upsilon - E_g\right) \qquad (3)$$

where A is a constant and n is equal to 2 for semiconductors with direct allowed transitions [87]. As shown by the inset graph in **Figure 6**, the value of E_g can be determined by extrapolating the linear part of the function curve with the energy axis. The estimated bandgap energy is 3.26 eV for ZnO nanostructures obtained at 700 °C, which is consistent with the values reported in the literature [52, 88].

3.2 Fabrication of energy harvesting devices

3.2.1 Characterization of the PDMS/ZnO composite films

Composites of porous ZnO nanostructures embedded in PDMS (PDMS/ZnO films) were fabricated. The composites were produced with a micro-structuring and in an unstructured form. SEM images of a micro-structured porous PDMS/ZnO film are presented in **Figure 7(a)**. The array of aligned cones observed has an average height of 380 μm, an average diameter of 300 μm, and a gap around 100 μm. **Figure 7(b)** combines the XRD diffractogram of the porous ZnO nanostructures, the PDMS/ZnO composite film, and the pure PDMS film. As expected, even if presenting a much lower intensity, the hexagonal wurtzite ZnO structure (ICDD 36–1451) can be identified in the PDMS/ZnO composite, whereas the PDMS film presents an amorphous structure.

3.2.2 Performance of the PDMS/ZnO nanogenerators

To optimize the nanogenerator output, its performance was evaluated by varying the concentration of the porous ZnO nanostructures in the PDMS film. This study was performed with unstructured composites. Three concentrations were considered to produce the devices: 20, 25, and 30 wt%. **Figure 8(a)** presents the peak-to-peak output voltage of the nanogenerators. The electrical characterization of the nanogenerators was performed by applying a mechanical stimulus with a pushing force of 2.3 N at frequency of 2 pushes per second with a home-made
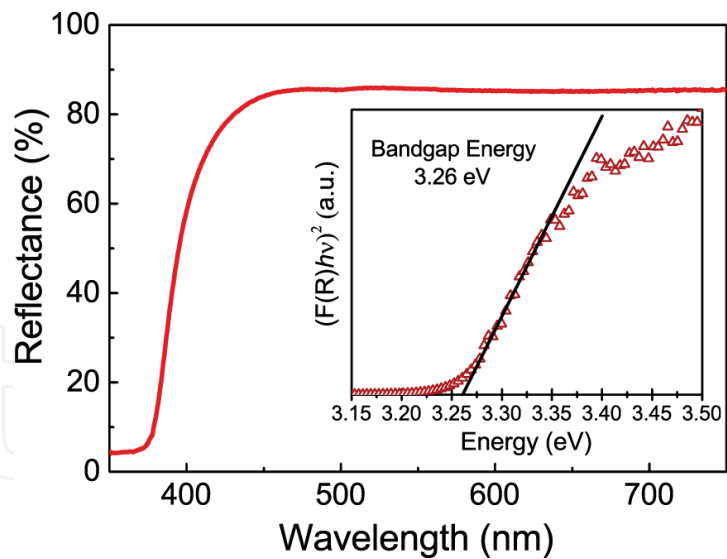
Figure 6.
Reflectance spectra of the porous ZnO nanostructures with an inset graphic showing the obtained bandgap energy via the K-M function.
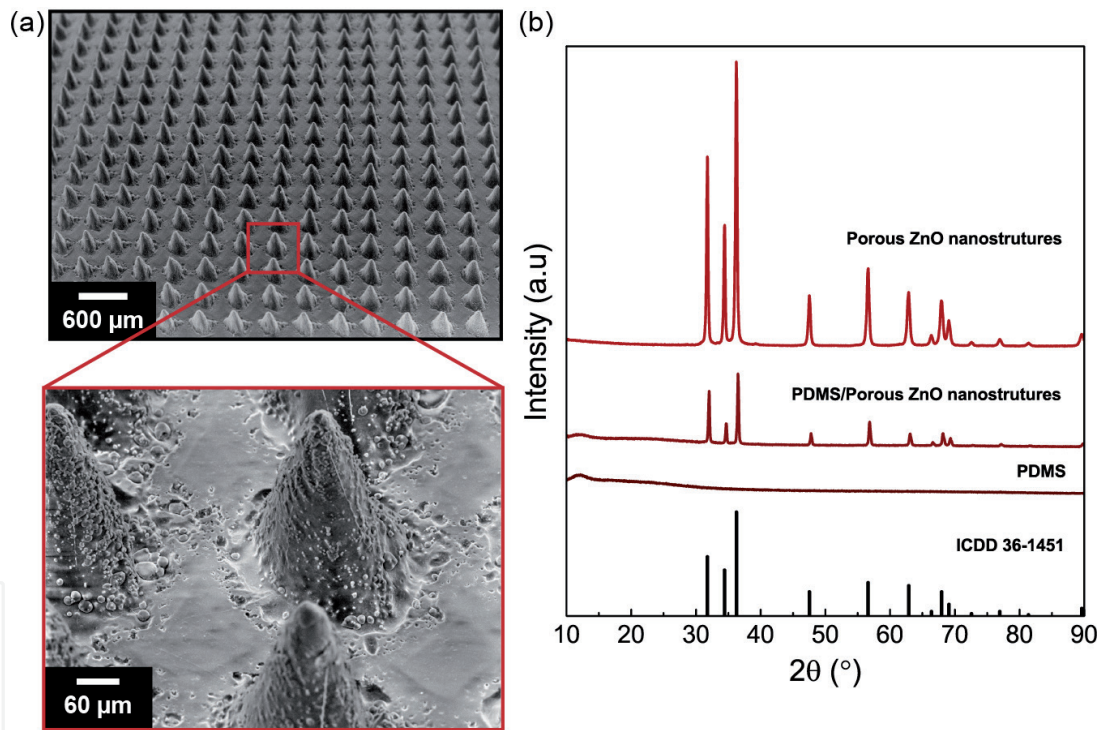

Figure 7.
(a) SEM images of a micro-structured PDMS/ZnO composite film, with the insets displaying closer views of the micro-cones. (b) XRD diffractogram of porous ZnO nanostructures, PDMS/ZnO composite film, and PDMS film.

bending machine. The obtained results reveal an increase of the output voltage from 20 to 25 wt%, and then a decrease for 30 wt%. These results are in agreement to what was previously observed using the same approach for ZnO nanorods, where the optimal concentration for the nanogenerators output was also 25 wt% [78]. As such, to further characterize the nanogenerators, the concentration considered was 25 wt%.

In previous studies from our group [27, 78], an enhanced response was achieved by micro-structuring the composite, as shown in **Figure 7**, and, therefore, the same approach was adopted in this study. **Figure 8(b)** presents the output voltage
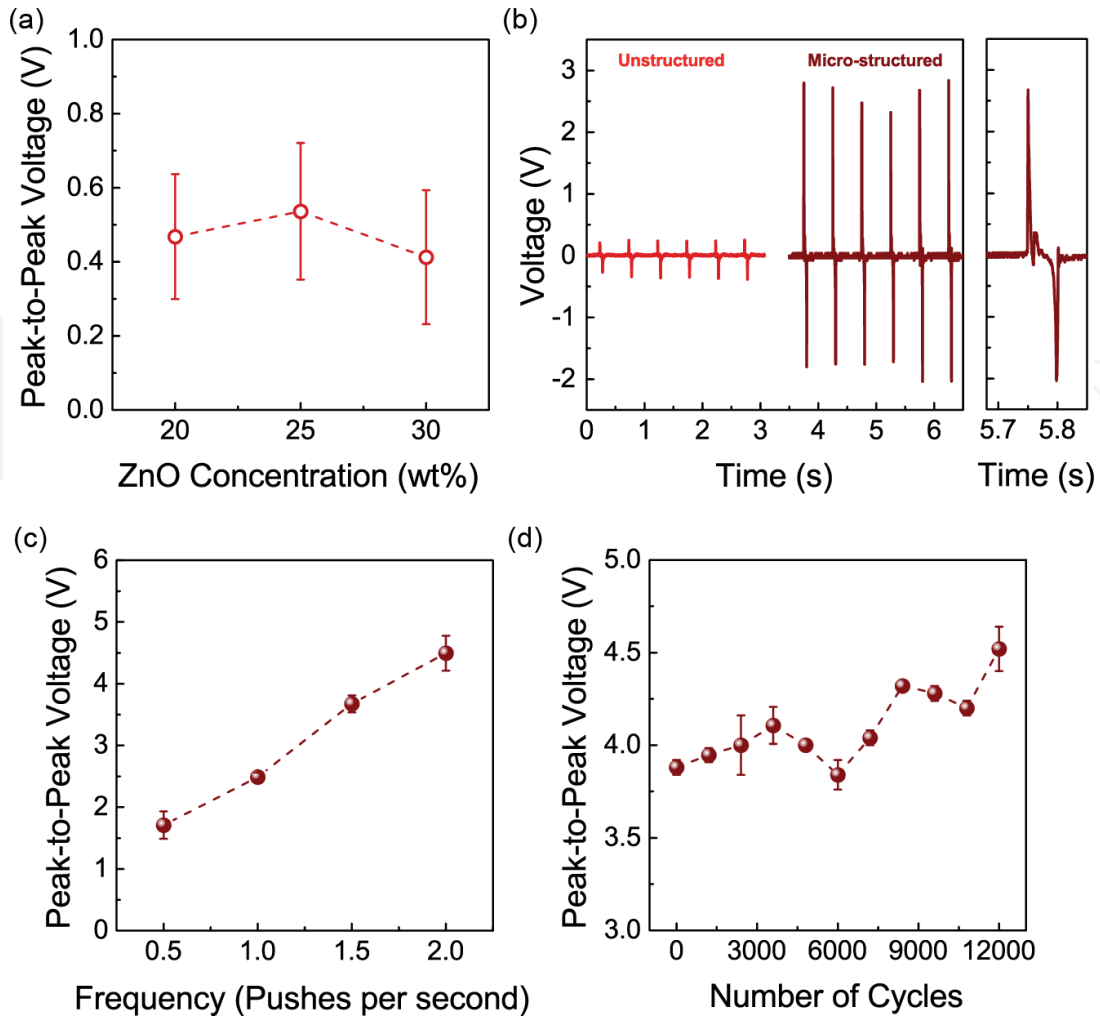
Figure 8.
(a) Peak-to-peak output voltage for PDMS/ZnO composites with different concentrations of porous ZnO nanostructures. Note that each point was determined using the average output of 2–6 equal devices. (b) Output voltage for an unstructured and a micro-structured nanogenerator with a porous ZnO nanostructures concentration of 25 wt%. (c) Peak-to-peak voltage for different frequencies applying a pushing force of 2.3 N. (d) Output voltage from the optimized nanogenerator for 12,000 cycles.

for this nanogenerator in comparison with the unstructured one. A peak-to-peak output voltage of (4.5 ± 0.3) V was obtained for the micro-structured nanogenerator against only (0.5 ± 0.2) V for the unstructured one. The micro-structuring can not only improve the force delivery into the nanostructures, leading to an increase of the piezoelectric effect, but it can also induce an extra triboelectric effect, as a consequence of the air gaps between the PDMS/ZnO composite micro-structures and the ITO electrode. These two effects originate an enhanced response of the micro-structured nanogenerator.

Considering the micro-structured nanogenerator with the best performance (25 wt%), the influence of varying the frequency of the stimulus was investigated while maintaining the applied force at 2.3 N. **Figure 8(c)** shows the peak-to-peak output voltage of the nanogenerator as function of the frequency, where the output voltage increases with increasing frequency. This trend has been observed by other groups, and it can be explained by the eventual accumulation of residual charges due to an inefficient neutralization of the induced charges provoked by a faster stimulation [89].

To study the potential of the nanogenerator in a daily life application, its stability along 12,000 cycles was also investigated. For this study, the stimulus was applied with a pushing force of 2.3 N while maintaining the frequency at 2 pushes per second. **Figure 8(d)** shows the output voltage along the pushing cycles, and no

deterioration of its performance is observed. Instead, it is possible to detect a slight increase of the output voltage to (7.2 ± 0.1) V along the pushing cycles, which can also be related to charges accumulation.

3.2.3 Proof-of-concept of the PDMS/ZnO nanogenerator

To understand the applicability of the micro-structured PDMS/ZnO nano-generator, it is important to study its performance when connected to external load resistances with different values (1 to 30 MΩ). This study was performed with a fixed pushing of 2.3 N at 2 pushes per second. **Figure 9(a)** presents the peak-to-peak output voltage and current, while **Figure 9(b)** shows the resultant instantaneous power density. An increase of the power density with increasing load resistance is observed until 10 MΩ, reaching a maximum value of 2.7 µW cm^{-2}, after that a slight decrease is observed. Comparing to the recent results on PDMS/ZnO nanorods nanogenerators [78], the maximum power obtained here is just slightly lower, presenting the same order of magnitude. Its lower output is expected due the absence of a preferential direction for piezo-electric response (c-axes) in these nanostructures. Nevertheless, the synthesis of these porous ZnO nanostructures allows for a faster and low-cost fabrication of nanogenerators, since it is a rapid, simple, and high yield approach to obtain ZnO nanostructures.

Additionally, the nanogenerator output is very satisfactory, proven to be enough to light up a blue LED (2.8–4 V, 20 mA), by directly connecting the nano-generator to the LED and manually stimulating the energy harvester, as shown in **Figures 9(c)** and **(d)** and Video 1 available from (can be viewed at) https://youtu.be/JCT60ozKCX8. These results prove not only the applicability of these
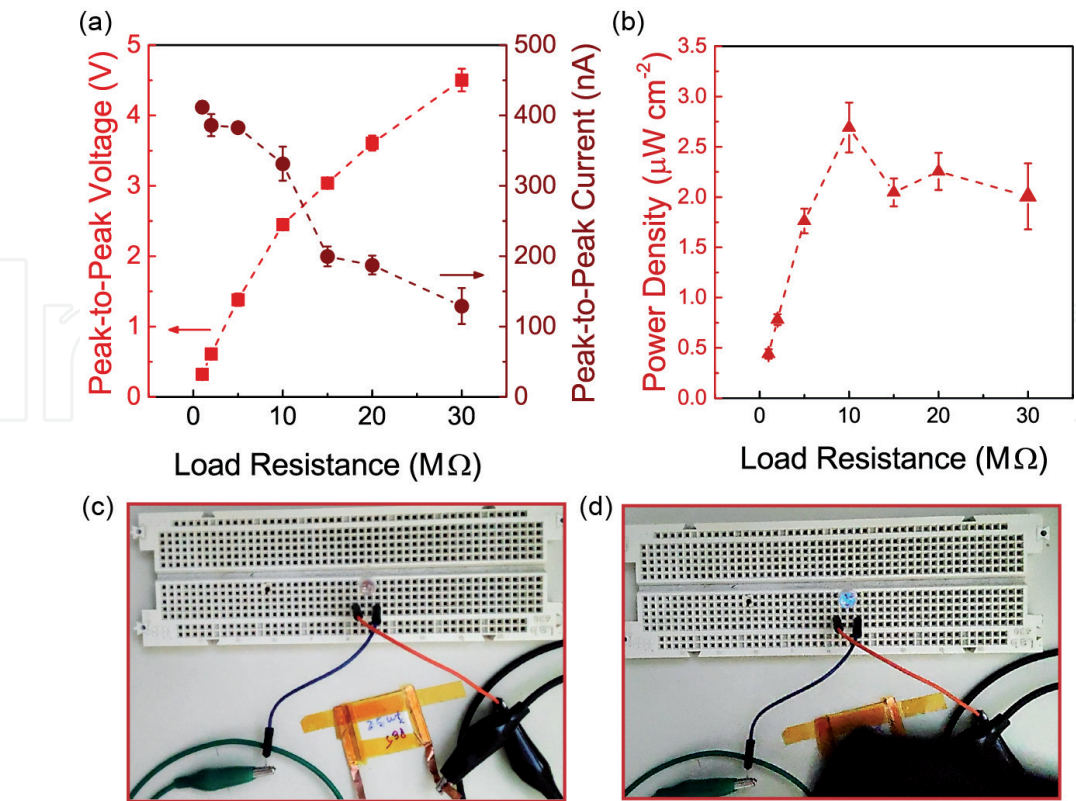
Figure 9.
Application of the micro-structured PDMS/ZnO nanogenerator, stimulated with a pushing force of 2.3 N at a frequency of 2 pushes per second varying the load resistance. Peak-to-peak (a) voltage and current outputs, and (b) correspondent power density for several load resistances. Note that each peak-to-peak value is an average of 5 measurements. (c and d) Nanogenerator directly lighting up a blue LED by applying manual force.

nanogenerators in simple daily life applications but also demonstrate their potential to power wearable sensors or multifunctional platforms where these porous ZnO nanostructures are employed in more than one application.

4. Conclusions

In summary, porous ZnO nanostructures were successfully synthesized via a facile and fast hydrothermal method assisted by microwave irradiation and calcinated at 700 °C for 2 h in air. The effect of calcination temperature on the morphological, structural, and optical properties of the porous ZnO nanostructures was investigated. Nanogenerators based on a micro-structured composite of PDMS with embedded porous ZnO structures were successfully produced, reaching an output voltage of (4.5 ± 0.3) V. The devices proved to be very robust and stable by presenting no deterioration of their performance after 12,000 pushing cycles. An external load of 10 MΩ optimized the nanogenerators performance, reaching a power density of 2.7 µW cm^{-2}. The capability of these nanogenerators to lighting up commercial LEDs, through direct connection and with a manual stimulus, was shown, demonstrating their potential for daily life applications.

Acknowledgements

Conflict of interest

The authors declare no conflict of interest.

Notes/thanks/other declarations

The authors would like to thank Ana Pimentel for the TG-DSC measurement and Daniela Nunes for the SEM images.

Author details

Sofia Henriques Ferreira*, Ana Rovisco*, Andreia dos Santos, Hugo Águas,
Rui Igreja, Pedro Barquinha, Elvira Fortunato and Rodrigo Martins*
CENIMAT/i3N, Department of Materials Science, NOVA School of Science and
Technology (FCT-NOVA) and CEMOP/UNINOVA, NOVA University Lisbon,
Caparica, Portugal

*Address all correspondence to: sdl.ferreira@campus.fct.unl.pt;
a.rovisco@campus.fct.unl.pt and rm@uninova.pt

IntechOpen

References

[1] Wojnarowicz J, Chudoba T, Lojkowski W. A Review of Microwave Synthesis of Zinc Oxide Nanomaterials : Reactants , Process Parameters and Morphologies. Nanomaterials. 2020;10:1086.

[2] Wang ZL. Zinc oxide nano structures: Growth, properties and applications. J Phys Condens Matter. 2004;16:R829–R858.

[3] Samouco A, Marques AC, Pimentel A, Martins R, Fortunato E. Laser-induced electrodes towards low-cost flexible UV ZnO sensors. Flex Print Electron. 2018;3:No. 044002.

[4] Ferreira SH, Deuermeier J, Sequeira S, Nunes D, Gonçalves AMF, Martins R, et al. Industrial waste residue converted into value-added ZnO for optoelectronic applications. ACS Appl Electron Mater. 2020;2(7):1960-1969.

[5] Lyubchyk A, Vicente A, Soule B, Alves PU, Mateus T, Mendes MJ, et al. Mapping the Electrical Properties of ZnO-Based Transparent Conductive Oxides Grown at Room Temperature and Improved by Controlled Postdeposition Annealing. Adv Electron Mater. 2016;2:1500287.

[6] Fortunato E, Fortunato E, Nunes P, Nunes P, Marques a, Marques a, et al. Transparent, conductive ZnO:Al thin film deposited on polymer substrates by RF magnetron sputtering. Science (80-). 2002;152:247-51.

[7] Zhu L, Zeng W. Room-temperature gas sensing of ZnO-based gas sensor: A review. Sensors Actuators, A Phys. 2017;267:242-261.

[8] Sun Y, Maemoto T, Sasa S. Fully transparent ZnO thin-film transistors using conducting AZO films fabricated at room temperature. 2014;2-3.

[9] Fortunato EMC, Barquinha PMC, Pimentel ACMBG, Gonçalves AMF, Marques AJS, Pereira LMN, et al. Fully transparent ZnO thin-film transistor produced at room temperature. Adv Mater. 2005;17:590-594.

[10] Muchuweni E, Sathiaraj TS, Nyakotyo H. Hydrothermal synthesis of ZnO nanowires on rf sputtered Ga and Al co-doped ZnO thin films for solar cell application. J Alloys Compd. 2017;721:45-54.

[11] Cao J, Wu B, Chen R, Wu Y, Hui Y, Mao BW, et al. Efficient, Hysteresis-Free, and Stable Perovskite Solar Cells with ZnO as Electron-Transport Layer: Effect of Surface Passivation. Adv Mater. 2018;30(11):1-9.

[12] Nayeri FD, Soleimani EA, Salehi F. Synthesis and characterization of ZnO nanowires grown on different seed layers: The application for dye-sensitized solar cells. Renew Energy. 2013;60:246-255.

[13] Özgür Ü, Alivov YI, Liu C, Teke a., Reshchikov M a., Doğan S, et al. A comprehensive review of ZnO materials and devices. J Appl Phys. 2005;98(4):1-103.

[14] Ong CB, Ng LY, Mohammad AW. A review of ZnO nanoparticles as solar photocatalysts: Synthesis, mechanisms and applications. Renew Sustain Energy Rev. 2018;81(March 2017):536-551.

[15] Samadi M, Zirak M, Naseri A, Khorashadizade E, Moshfegh AZ. Recent progress on doped ZnO nanostructures for visible-light photocatalysis. Thin Solid Films. 2016;605:2-19.

[16] Pimentel A, Rodrigues J, Duarte P, Nunes D, Costa FM, Monteiro T, et al. Effect of solvents on ZnO nanostructures synthesized

by solvothermal method assisted by microwave radiation: a photocatalytic study. J Mater Sci. 2015;50:5777-5787.

[17] Theerthagiri J, Salla S, Senthil RA, Nithyadharseni P, Madankumar A, Arunachalam P, et al. A review on ZnO nanostructured materials : energy, environmental and biological applications. Nanotechnology. 2019;30:392001.

[18] Rong P, Ren S, Yu Q. Fabrications and Applications of ZnO Nanomaterials in Flexible Functional Devices-A Review. Crit Rev Anal Chem. 2019;49(4):336-349.

[19] Sanguino P, Monteiro T, Bhattacharyya SR, Dias CJ, Igreja R, Franco R. ZnO nanorods as immobilization layers for interdigitated capacitive immunosensors. Sensors Actuators, B Chem. 2014;204:211-217.

[20] Askari H, Khajepour A, Khamesee MB, Saadatnia Z, Wang ZL. Piezoelectric and triboelectric nanogenerators: Trends and impacts. Nano Today. 2018 Oct;22(1):10-13.

[21] Wang ZL. Nanogenerators for Self-powered Devices and Systems. 2011.

[22] Indira SS, Vaithilingam CA, Oruganti KSP, Mohd F, Rahman S. Nanogenerators as a sustainable power source: state of art, applications, and challenges. Nanomaterials. 2019;9(5):773.

[23] Safari A, Akdogan EK. Piezoelectric and Acoustic Materials for Transducer Applications. 2008.

[24] Ibn-Mohammed T, Reaney IM, Koh SCL, Acquaye A, Sinclair DC, Randall CA, et al. Life cycle assessment and environmental profile evaluation of lead-free piezoelectrics in comparison with lead zirconate titanate. J Eur Ceram Soc. 2018;38:4922-4938.

[25] Fan HJ, Lee W, Hauschild R, Alexe M, Rhun G Le, Scholz R, et al. Template-assisted large-scale ordered arrays of ZnO pillars for optical and piezoelectric applications. Small. 2006;2(4):561-568.

[26] Broitman E, Soomro MY, Lu J, Willander M, Hultman L. Nanoscale piezoelectric response of ZnO nanowires measured using a nanoindentation technique. Phys Chem Chem Phys. 2013 Jul;15(26):11113-11118.

[27] Rovisco A, dos Santos A, Cramer T, Martins J, Branquinho R, Águas H, et al. Piezoelectricity Enhancement of Nanogenerators Based on PDMS and ZnSnO 3 Nanowires through Microstructuration. ACS Appl Mater Interfaces. 2020 Apr;12(16):18421-18430.

[28] Shetti NP, Bukkitgar SD, Reddy KR, Reddy CV, Aminabhavi TM. ZnO-based nanostructured electrodes for electrochemical sensors and biosensors in biomedical applications. Biosens Bioelectron. 2019;141(March):111417.

[29] Yin B, Qiu Y, Zhang H, Lei J, Chang Y, Ji J, et al. Piezoelectric effect of 3-D ZnO nanotetrapods. RSC Adv. 2015;5(15):11469-11474.

[30] Wu JM, Xu C, Zhang Y, Yang Y, Zhou Y, Wang ZL. Flexible and transparent nanogenerators based on a composite of lead-free ZnSnO3 triangular-belts. Adv Mater. 2012;24(45):6094-6099.

[31] Guo R, Guo Y, Duan H, Li H, Liu H. Synthesis of Orthorhombic Perovskite-Type ZnSnO3 Single-Crystal Nanoplates and Their Application in Energy Harvesting. ACS Appl Mater Interfaces. 2017 Mar;9(9):8271-8279.

[32] Alam MM, Ghosh SK, Sultana A, Mandal D. Lead-free ZnSnO3/MWCNTs-based self-poled flexible hybrid nanogenerator for

piezoelectric power generation. Nanotechnology. 2015;26(16):165403.

[33] Choi KH, Siddiqui GU, Yang B, Mustafa M. Synthesis of ZnSnO3 nanocubes and thin film fabrication of (ZnSnO3/PMMA) composite through electrospray deposition. J Mater Sci Mater Electron. 2015;26:5690-5696.

[34] Paria S, Karan SK, Bera R, Das AK, Maitra A, Khatua BB. A Facile Approach To Develop a Highly Stretchable PVC/ZnSnO 3 Piezoelectric Nanogenerator with High Output Power Generation for Powering Portable Electronic Devices. Ind Eng Chem Res. 2016 Oct;55(40):10671-10680.

[35] Saravanakumar B, Mohan R, Thiyagarajan K, Kim SJ. Fabrication of a ZnO nanogenerator for eco-friendly biomechanical energy harvesting. RSC Adv. 2013;3(37):16646-16656.

[36] Rahman W, Garain S, Sultana A, Ranjan Middya T, Mandal D. Self-Powered Piezoelectric Nanogenerator Based on Wurtzite ZnO Nanoparticles for Energy Harvesting Application. Materials Today: Proceedings. 2018. p. 9826-9830.

[37] Kim DH, Dudem B, Yu JS. High-Performance Flexible Piezoelectric-Assisted Triboelectric Hybrid Nanogenerator via Polydimethylsiloxane-Encapsulated Nanoflower-like ZnO Composite Films for Scavenging Energy from Daily Human Activities. ACS Sustain Chem Eng. 2018;6(7):8525-8535.

[38] Manthina V, Agrios AG. Single-pot ZnO nanostructure synthesis by chemical bath deposition and their applications. Nano-Structures & Nano-Objects. 2016 Jul 1;7:1-11.

[39] Ait hssi A, Amaterz E, Labchir N, Atourki L, Bouderbala IY, Elfanaoui A, et al. Electrodeposited ZnO Nanorods as Efficient Photoanodes for the Degradation of Rhodamine B. Phys Status Solidi. 2020;217(17):2000349.

[40] Lupan O, Emelchenko GA, Ursaki V V., Chai G, Redkin AN, Gruzintsev AN, et al. Synthesis and characterization of ZnO nanowires for nanosensor applications. Mater Res Bull. 2010;45(8):1026-1032.

[41] Lin D, Wu H, Pan W. Photoswitches and memories assembled by electrospinning aluminum-doped zinc oxide single nanowires. Adv Mater. 2007;19(22):3968-3972.

[42] Rodrigues J, Fernandes AJS, Monteiro T, Costa FM. A review on the laser-assisted flow deposition method: growth of ZnO micro and nanostructures. CrystEngComm. 2019;21(7):1071-1090.

[43] Mahpeykar SM, Koohsorkhi J, Ghafoori-fard H. Ultra-fast microwave-assisted hydrothermal synthesis of long vertically aligned ZnO nanowires for dye-sensitized solar cell application. Nanotechnology. 2012;23(16):165602.

[44] Qiu Y, Chen W, Yang S. Facile hydrothermal preparation of hierarchically assembled, porous single-crystalline ZnO nanoplates and their application in dye-sensitized solar cells. J Mater Chem. 2010;20(5):1001-1006.

[45] Pimentel A, Nunes D, Duarte P, Rodrigues J, Costa FM, Monteiro T, et al. Synthesis of long ZnO nanorods under microwave irradiation or conventional heating. J Phys Chem C. 2014;118:14629-14639.

[46] Jang JS, Lee SE, Choi SJ, Koo WT, Kim DH, Shin H, et al. Heterogeneous, Porous 2D Oxide Sheets via Rapid Galvanic Replacement: Toward Superior HCHO Sensing Application. Adv Funct Mater. 2019;29(42):1-10.

[47] Huang A, He Y, Zhou Y, Zhou Y, Yang Y, Zhang J, et al. A review of recent

applications of porous metals and metal oxide in energy storage, sensing and catalysis. J Mater Sci. 2019;54(2):949-973.

[48] Sk MM, Yue CY, Ghosh K, Jena RK. Review on advances in porous nanostructured nickel oxides and their composite electrodes for high-performance supercapacitors. J Power Sources. 2016;308:121-140.

[49] Butburee T, Bai Y, Wang H, Chen H, Wang Z, Liu G, et al. 2D Porous TiO2 Single-Crystalline Nanostructure Demonstrating High Photo-Electrochemical Water Splitting Performance. Adv Mater. 2018;30(21):1-8.

[50] Xie X, Wang X, Tian J, Song X, Wei N, Cui H. Growth of porous ZnO single crystal hierarchical architectures with ultrahigh sensing performances to ethanol and acetone gases. Ceram Int. 2017;43(1):1121-1128.

[51] Jin Z, Zhang YX, Meng FL, Jia Y, Luo T, Yu XY, et al. Facile synthesis of porous single crystalline ZnO nanoplates and their application in photocatalytic reduction of Cr(VI) in the presence of phenol. J Hazard Mater. 2014;276:400-407.

[52] Liu S, Li C, Yu J, Xiang Q. Improved visible-light photocatalytic activity of porous carbon self-doped ZnO nanosheet-assembled flowers. CrystEngComm. 2011;13(7):2533-2541.

[53] Song B, Wang Y, Cui X, Kou Z, Si L, Tian W, et al. A Series of Unique Architecture Building of Layered Zinc Hydroxides: Self-Assembling Stepwise Growth of Layered Zinc Hydroxide Carbonate and Conversion into Three-Dimensional ZnO. Cryst Growth Des. 2016;16(2):887-894.

[54] Zhang L, Zhao J, Lu H, Li L, Zheng J, Li H, et al. Facile synthesis and ultrahigh ethanol response of

hierarchically porous ZnO nanosheets. Sensors Actuators, B Chem. 2012;161(1):209-215.

[55] Moezzi A, Cortie M, McDonagh A. Transformation of zinc hydroxide chloride monohydrate to crystalline zinc oxide. Dalt Trans. 2016;45(17):7385-7390.

[56] Moezzi A, Cortie MB, McDonagh AM. Zinc hydroxide sulphate and its transformation to crystalline zinc oxide. Dalt Trans. 2013;42(40):14432-14437.

[57] Hosono E, Fujihara S, Kimura T, Imai H. Growth of layered basic zinc acetate in methanolic solutions and its pyrolytic transformation into porous zinc oxide films. J Colloid Interface Sci. 2004;272(2):391-398.

[58] Song RQ, Xu AW, Deng B, Li Q, Chen GY. From layered basic zinc acetate nanobelts to hierarchical zinc oxide nanostructures and porous zinc oxide nanobelts. Adv Funct Mater. 2007;17(2):296-306.

[59] Li B, Wang Y. Hierarchically assembled porous ZnO microstructures and applications in a gas sensor. Superlattices Microstruct. 2011;49(4):433-440.

[60] Mao J, Li JJ, Ling T, Liu H, Yang J, Du XW. Facile synthesis of zinc hydroxide carbonate flowers on zinc oxide nanorods with attractive luminescent and optochemical performance. Nanotechnology. 2011;22(24):245607.

[61] Chen M, Wang Z, Han D, Gu F, Guo G. Porous ZnO polygonal nanoflakes: Synthesis, use in high-sensitivity NO 2 gas sensor, and proposed mechanism of gas sensing. J Phys Chem C. 2011;115(26):12763-12773.

[62] Bitenc M, Marinšek M, Crnjak Orel Z. Preparation and characterization

of zinc hydroxide carbonate and porous zinc oxide particles. J Eur Ceram Soc. 2008;28(15):2915-2921.

[63] Gu F, You D, Wang Z, Han D, Guo G. Improvement of gas-sensing property by defect engineering in microwave-assisted synthesized 3D ZnO nanostructures. Sensors Actuators, B Chem. 2014;204(3):342-350.

[64] Zhang Y, Liu C, Gong F, Jiu B, Li F. Large scale synthesis of hexagonal simonkolleit nanosheets for ZnO gas sensors with enhanced performances. Mater Lett. 2017;186(August 2016):7-11.

[65] Teng Y, Mo M, Li Y, Xue J, Zhao H. Amorphous carbon-coated ZnO porous nanosheets: Facile fabrication and application in lithium- and sodium-ion batteries. J Alloys Compd. 2018;744:712-720.

[66] Shinagawa T, Watanabe M, Mori T, Tani JI, Chigane M, Izaki M. Oriented Transformation from Layered Zinc Hydroxides to Nanoporous ZnO: A Comparative Study of Different Anion Types. Inorg Chem. 2018;57(21):13137-13149.

[67] Pimentel A, Nunes D, Pereira S, Martins R, Fortunato E. Photocatalytic Activity of TiO2 Nanostructured Arrays Prepared by Microwave-Assisted Solvothermal Method. Cao W, editor. Semiconductor Photocatalysis - Materials, Mechanisms and Applications. 2016. p. 81-103.

[68] Hayes BL. Microwave Synthesis: Chemistry at the Speed of Light. 2002.

[69] Mirzaei A, Neri G. Microwave-assisted synthesis of metal oxide nanostructures for gas sensing application: A review. Sensors Actuators, B Chem. 2016;237:749-775.

[70] Liu D, Lv Y, Zhang M, Liu Y, Zhu Y, Zong R, et al. Defect-related photoluminescence and photocatalytic

properties of porous ZnO nanosheets. J Mater Chem A. 2014;2(37):15377-15388.

[71] Zhou J, Gong F, Wang H, Xiao Y, Li F, Mai W. 3D mace-like hierarchical ZnO nanoarchitecture constructed with microrod bundles and porous single-crystalline nanosheets for acetone sensors with enhanced performances. Mater Sci Eng B Solid-State Mater Adv Technol. 2017;225(May):68-74.

[72] Lin Z, Guo F, Wang C, Wang X, Wang K, Qu Y. Preparation and sensing properties of hierarchical 3D assembled porous ZnO from zinc hydroxide carbonate. RSC Adv. 2014;4(10):5122-5129.

[73] Chang J, Ahmad MZ, Wlodarski W, Waclawik ER. Self-assembled 3D ZnO porous structures with exposed reactive {0001} facets and their enhanced gas sensitivity. Sensors. 2013;13(7):8445-8460.

[74] Yang H, Ni S-Q, Jiang X, Jiang W, Zhan J. In situ fabrication of single-crystalline porous ZnO nanoplates on zinc foil to support silver nanoparticles as a stable SERS substrate. CrystEngComm. 2012;14(18):6023.

[75] Lai YH, Lin CY, Chen HW, Chen JG, Kung CW, Vittal R, et al. Fabrication of a ZnO film with a mosaic structure for a high efficient dye-sensitized solar cell. J Mater Chem. 2010;20(42):9379-9385.

[76] Hosono E, Fujihara S, Honma I, Zhou H. The fabrication of an upright-standing zinc oxide nanosheet for use in dye-sensitized solar cells. Adv Mater. 2005;17(17):2091-2094.

[77] Zhang XS, Han M Di, Wang RX, Zhu FY, Li ZH, Wang W, et al. Frequency-multiplication high-output triboelectric nanogenerator for sustainably powering biomedical microsystems. Nano Lett. 2013;13(3):1168-1172.

[78] dos Santos A, Sabino F, Rovisco A, Barquinha P, Águas H, Fortunato E, et al. Optimization of ZnO Nanorods Concentration in a Micro-Structured Polymeric Composite for Nanogenerators. Chemosensors. 2021 Jan;9(2):27.

[79] dos Santos A, Pinela N, Alves P, Santos R, Fortunato E, Martins R, et al. Piezoresistive E-Skin Sensors Produced with Laser Engraved Molds. Adv Electron Mater. 2018;4(9):1800182-1800192.

[80] Jing Z, Zhan J. Fabrication and Gas-Sensing Properties of Porous ZnO Nanoplates. Adv Mater. 2008;(20):4547-4551.

[81] Liu X, Zhang J, Wang L, Yang T, Guo X, Wu S, et al. 3D hierarchically porous ZnO structures and their functionalization by Au nanoparticles for gas sensors. J Mater Chem. 2011;21(2):349-356.

[82] Yang H, Ni SQ, Jiang X, Jiang W, Zhan J. In situ fabrication of single-crystalline porous ZnO nanoplates on zinc foil to support silver nanoparticles as a stable SERS substrate. CrystEngComm. 2012;14(18):6023-6028.

[83] Xingfu Z, Zhaolin H, Yiqun F, Su C, Weiping D, Nanping X. Microspheric organization of multilayered ZnO nanosheets with hierarchically porous structures. J Phys Chem C. 2008;112(31):11722-11728.

[84] Wang X, Cai W, Lin Y, Wang G, Liang C. Mass production of micro/nanostructured porous ZnO plates and their strong structurally enhanced and selective adsorption performance for environmental remediation. J Mater Chem. 2010;20(39):8582-8590.

[85] Mishra V, Warshi MK, Sati A, Kumar A, Mishra V, Sagdeo A, et al. Diffuse reflectance spectroscopy: An effective tool to probe the defect states in wide band gap semiconducting materials. Mater Sci Semicond Process. 2018;86:151-156.

[86] Akir S, Barras A, Coffinier Y, Bououdina M, Boukherroub R, Omrani AD. Eco-friendly synthesis of ZnO nanoparticles with different morphologies and their visible light photocatalytic performance for the degradation of Rhodamine B. Ceram Int. 2016;42(8):10259-10265.

[87] Viezbicke BD, Patel S, Davis BE, Birnie DP. Evaluation of the Tauc method for optical absorption edge determination: ZnO thin films as a model system. Phys Status Solidi Basic Res. 2015;252(8):1700-1710.

[88] Huang N, Shu J, Wang Z, Chen M, Ren C, Zhang W. One-step pyrolytic synthesis of ZnO nanorods with enhanced photocatalytic activity and high photostability under visible light and UV light irradiation. J Alloys Compd. 2015;648:919-929.

[89] Ko YH, Nagaraju G, Lee SH, Yu JS. PDMS-based Triboelectric and Transparent Nanogenerators with ZnO Nanorod Arrays. ACS Appl Mater Interfaces. 2014 May;6(9):6631-6637.